Interfacial oxygen nanobubbles reduce methylmercury production ability of sediments in eutrophic waters

Xiaonan Ji[1,2], Chengbin Liu[1,3], Gang Pan*[1,2,4,5]

[1] *Research Center for Eco-Environmental Sciences, Chinese Academy of Sciences, Beijing, 100085, PR China*

[2] *University of Chinese Academy of Sciences, Beijing, 100049, PR China*

[3] *State Key Laboratory of Pollution Control and Resource Reuse, College of Environmental Science and Engineering, Tongji University, 1239 Siping Road, Shanghai 200092, PR China*

[4] *Beijing Advanced Science and Innovation Center, Chinese Academy of Sciences, Beijing, 101407, PR China*

[5] *Center of Integrated Water-Energy-Food studies (iWEF), School of Animal, Rural, and Environmental Sciences, Nottingham Trent University, Brackenhurst Campus NG25 0QF, UK*

* Corresponding author. Research Center for Eco-Environmental Sciences, Chinese Academy of Sciences, Beijing, 100085, PR China.

Email address: gpan@rcees.ac.cn (G. Pan)

Abstract

Eutrophication can induce hypoxia/anoxia and rich organic matter at the sediment-water interface in surface waters. When eutrophic waters are impacted with mercury (Hg) pollution, methylmercury (MeHg) production ability (MPA) of surface sediment would increase and more MeHg might be produced. To tackle this risk, this study firstly collected samples of surface sediment and overlying water from a typical eutrophic lake—Taihu Lake. Then from a sediment-water simulation system, we demonstrated that eutrophic waters were able to methylate Hg spontaneously, and that sediment is the major Hg sink in the system. After the addition of $HgCl_2$ solution (approximately 1 mg L^{-1} in the slurry), MeHg concentrations in the sediment increased by 11.7 times after 48 h. The subsequent column experiments proved that O_2 nanobubbles could significantly decrease the MPA of surface sediment, by up to 48%. Furthermore, we found that O_2 nanobubbles could remediate anoxia mainly by increasing dissolved oxygen (from 0 to 2.1 mg L^{-1}), oxidation-reduction potentials (by 37% on average), and sulfate (by 31% on average) in the overlying water. In addition, O_2 nanobubbles could also help decrease organic matter concentration, as was revealed by the decline of dissolved organic carbon in the overlying water (by up to 57%) and total organic carbon in surface sediment (by up to 37%). The remediation of anoxia and reduction of organic matter could contribute to the decrease of *hgcA* gene abundance (by up to 86%), and thus result in the reduction of MPA after the addition of O_2 nanobubbles. This study revealed the risk of MeHg production in case Hg pollution occurs in eutrophic waters and proposed a feasible solution for MeHg remediation.

Keywords: Mercury pollution; Mercury methylation; Anoxia remediation; Organic matter; Mercury microbial methylator

1. Introduction

Mercury (Hg) is a toxic trace metal that can travel globally in atmosphere and enter hydrosphere by deposition (Krabbenhoft and Sunderland, 2013). Human activities, such as chlor-alkali production, fossil-fuel combustion, and mining, have greatly augmented Hg flux into aquatic system (Streets et al., 2011). It is suggested that anthropogenic perturbations have tripled Hg content in surface waters since industrialization (Lamborg et al., 2014). Hg pollution in aquatic environment is emerging globally, either in oceans (Mason, 2013; Sunderland et al., 2009; Gobeil et al., 1999) or in freshwaters (Li et al., 2012; Li et al., 2009; Jiang et al., 2006). In addition, Hg content in the sediment far exceeds that in the overlying water. Particularly, certain Hg-contaminated sediments in urban, industrial, or mineralized areas might exhibit high Hg concentrations, some of which could reach up to several hundred μg Hg g^{-1} (Liu et al., 2017; Feng et al., 2006).

In surface waters, inorganic Hg can be methylated to methylmercury (MeHg), whose content corresponds with changes of Hg inputs (Harris et al., 2007). As a potential neurotoxin, MeHg can pose a significant health threat to human beings after bioaccumulation and biomagnification (Gilmour et al., 2013). Hg methylation is primarily mediated by anaerobic bacteria carrying *hgcAB* genes, such as sulfate-reducing bacteria, and tends to take place in anaerobic conditions (Parks et al., 2013). In addition, organic matter can facilitate the production of MeHg by acting as electron donor and microbial substrate for Hg microbial methylators (Bravo et al., 2017; Gu et al., 2011). It has been reported that niches like aquatic sediments are hotspot areas for MeHg production (Podar et al., 2015). For instance, sediments are able to produce high levels of MeHg if the watershed is impacted with Hg pollution

(Balogh et al., 2015; Hachiya, 2012). Generally in sediments, the maximum Hg methylation rates appear at the surface layer (Ullrich et al., 2001).

To evaluate MeHg production in different environmental matrices, indexes such as Hg methylation rate constant and ratio of MeHg to total mercury (THg) have been used in a previous study (Drott et al., 2008). Yet, these indexes are less likely to reflect net MeHg production if Hg pollution occurs in different environment niches. Herein, MeHg production ability (MPA) is proposed as an indicator to quantify environmental matrix's ability to produce MeHg after exogenous Hg input. It is calculated as the increase of MeHg concentration after 48 h divided by the initial Hg ion (Hg^{2+}) concentration. Accordingly, areas with high MPAs should be paid close attention to for having substantial risks of MeHg production when Hg pollution occurs.

Eutrophication is a widespread water pollution in surface waters, affecting 58% of global lakes since industrialization (Taranu et al., 2015). In eutrophic waters, cyanobacteria can form dense blooms and induce adverse effects on the aquatic ecosystems (Huisman et al., 2018). The degradation of cyanobacterial blooms requires oxygen (O_2) and could lead to a state of hypoxia or anoxia in the system (Wang et al., 2016a). Then the subsequent deposition of the degraded cyanobacteria could result in the accumulation of organic matter on the surface sediment (Conley et al., 2009). As a result, in eutrophic waters, surface sediment is likely to display high MPA (Lei et al., 2019). Furthermore, in hyper-eutrophic waters, cyanobacterial blooms might evolve into black blooms, which could further aggravate hypoxia/anoxia in the system. During the outbreak of black blooms, sulfate-reducing bacteria were suggested to be the primary biological factor (Feng et al., 2014), and

they also plays in major role in Hg methylation. Therefore, once impacted with exogenous Hg input, surface sediment in hyper-eutrophic waters is highly possible to produce massive MeHg, which requires immediate concern.

Several manipulations have been proposed for MeHg remediation in sediments. For instance, capping sorbents like biochar and activated carbon were evaluated for MeHg stabilization in sediments (Liu et al., 2017; Gilmour et al., 2013). Still, as pyrolyzed carbon, these sorbents are likely to release carbon to aquatic systems and might have unpredictable impacts on MeHg production in the long term (Gilmour et al., 2018; Liu et al., 2018a). In addition, aeration of the anoxic sediment has also been proposed to inhibit MeHg production by eliminating hypoxia/anoxia. Nevertheless, the technical feasibility and economic pressure have been a concern due to the large volume of oxygen required (Mailman et al., 2006). Moreover, the subsequent vertical mixing might result in the release of MeHg from sediment to overlying waters as well, which could do greater harm to the aquatic organisms (Soerensen et al., 2016).

Interfacial nanobubbles are nanobubbles with radius of curvature of 100–1000 nm and mainly produced at the solid-liquid interface (Seddon et al., 2012). With nanoscale sizes, interfacial nanobubbles can exhibit unique characteristics like extended lifetime and great gas solubility. Interfacial oxygen nanobubbles can be loaded on natural zeolites (specific gravity of 2.15–2.25 g cm^{-3}), which are persistent clay minerals and unlikely to add extra ecological pressure to aquatic ecosystems (Lyu et al., 2019). Moreover, oxygen nanobubble-loaded zeolites can settle naturally to the designated areas like surface sediment, at which they can release oxygen to remediate hypoxia/anoxia (Shi et al., 2018). As Hg methylation

tends to occur in the anaerobic conditions, the mitigation of hypoxia/anoxia by O_2 nanobubbles might induce a reduction in the MPA of surface sediment. Therefore, interfacial oxygen nanobubble (loaded on zeolites) might provide a feasible solution for MeHg remediation in surface sediment.

In this work, we performed the Hg methylation and MPA mitigation experiments to investigate the reduction effects of interfacial O_2 nanobubbles on the probably increased MPA of surface sediment, in case severe Hg pollution occurs in eutrophic waters. Our primary objectives are firstly to reveal the fate of THg and MeHg in eutrophic waters impacted with Hg pollution, and to determine the optimal conditions for MPA analysis; secondly, to examine the effects of interfacial O_2 nanobubbles on MPA of surface sediment; finally, to elucidate the mechanism of the mitigation effects of interfacial O_2 nanobubbles.

2. Materials and methods

2.1 Sampling site

The samples of overlying water and surface sediment were collected from an algae accumulation zone in Meiliang Bay (120°09' E, 31°31' N), north of Taihu Lake in December of 2016 and September of 2017. Spatial distribution of the sampling sites is shown in **Fig. S1** in the Supplementary information (SI). Taihu Lake is a typical eutrophic shallow lake located in Wuxi City, Jiangsu Province (China). In recent decades, it has been suffering from severe cyanobacterial blooms nearly every summer (Wang et al., 2016b). Once collected, samples of overlying water and surface sediment were sealed and transferred to the lab at 4 ℃ in the dark instantly.

2.2 Experimental design

The scheme of the whole experimental design is illustrated in **Fig. 1**. The experiment is composed of two phases. The first phase is the Hg methylation experiment performed in 8 mL amber glass vials with lake sediment and water (**Fig. 1A**). It is designed to determine the optimal dosage of $HgCl_2$ solution and incubation time for MPA analysis. In brief, the MPA was calculated by the ratio of the changes in MeHg concentrations after 48h to the initial Hg^{2+} concentrations (more details refer to Section 2.5). The second phase is the MPA mitigation experiment, which combines sediment-water column experiment and MPA analysis in surface sediment from the columns (**Fig 1B**).

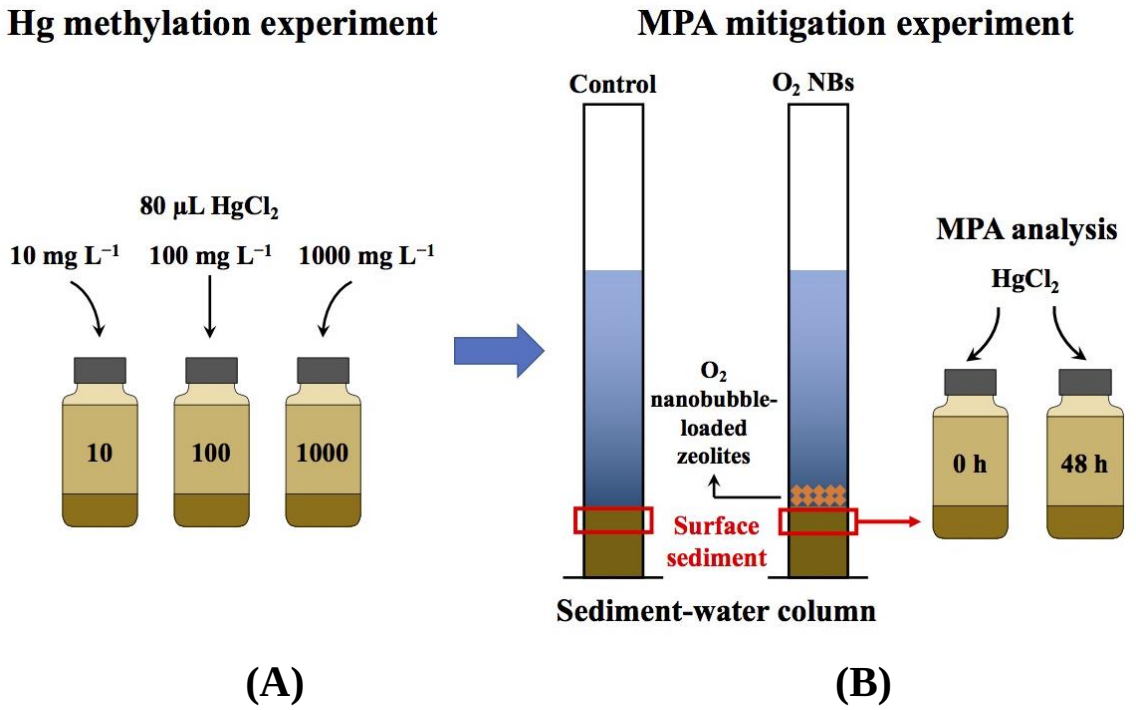

Fig. 1. Scheme of the whole experimental design. The experiment is composed of two phases: (A) The Hg methylation experiment. (B) The MPA mitigation experiment.

2.2.1 Hg methylation experiment

The Hg methylation experiment was carried out in a total of 48 amber glass vials of 8 mL (CNW, USA) with Teflon® lids. Approximately 110 g sediment were stirred with 330 mL deoxygenated lake water (1:3, m:m), both of which were collected from Taihu Lake in 2016. Then aliquots of 8 mL were transferred to the vials and spiked with 80 µL of 10, 100, and 1000 mg L^{-1} $HgCl_2$ solutions, leaving the final $HgCl_2$ concentrations to be around 0.1, 1, and 10 mg L^{-1} in the slurries. The vials were then left to settle after homogenization and incubate in the dark at room temperature. At the same time each day during 7 days, two vials of each spiking concentration were sacrificed for THg and MeHg analysis. During sampling, the overlying water was extracted, filtered with 0.22 µm syringe filters (ANPEL Laboratory Technologies (Shanghai) Inc., China), then spiked with 30 µL concentrated hydrochloric acid, and stored at 4 ℃ for further analysis. The remaining sediment was frozen at −20 ℃ overnight and freeze dried before analysis. The Hg methylation experiment was carried out in an anaerobic box. All experiments were performed in duplicate.

2.2.2 MPA mitigation experiments

The MPA mitigation experiment was carried out in the plexiglass cylinder columns (Beijing Yinfan Yangming Environmental Protection Technology Co., Ltd., China), which were 5 cm in diameter and 50 cm in height. Each column was filled with 6 cm deep surface sediment and 20 cm deep lake water (ca. 400 mL) collected from Taihu Lake in 2017. The columns were sealed with rubber plugs (applied with Vaseline) and Parafilm® M Film (Bemis Company, USA) and put in the dark at 25 ℃ (average temperature of Taihu Lake water in September) for 30 days without $HgCl_2$ addition to establish a steady sediment-water interface (Shen et al., 2003). During the last 7 days, dissolved oxygen (DO) concentrations (recorded

with a portable DO meter, SI) in the overlying water (about 2 cm above the sediment) maintained at 0. In the meantime, the overlying water in the columns started to turn grey and odorous, which is the typical sign of black blooms.

The columns were divided into two groups: i) the Control group was only filled with Taihu sediment and lake water; ii) the O_2 nanobubbles group (O_2 NBs) was based on the Control treatment and added with O_2 nanobubble-loaded zeolites. The preparation and characterization of O_2 nanobubble-loaded zeolites, discussed briefly in the SI, were described in Shi et al., 2018, Zhang et al. 2018 and Wang et al., 2018. and they were put to use immediately after preparation. On day 0 of the incubation of the columns, O_2 nanobubble-loaded zeolites (ca. 2 cm in height in the columns) were sprinkled evenly on the surface sediment of the O_2 NBs group. Then all the columns were sealed except when sampling or analyzing DO and oxidation-reduction potential (ORP) during the experiments. After the addition of O_2 nanobubble-loaded zeolites, the incubation of the columns began and lasted for 20 days.

1) MeHg production ability analysis

On days 2, 4, 8, 12, and 20 of the incubation, two columns of either treatment were sacrificed for the analysis of MPA and relevant physicochemical parameters. According to the results of the Hg methylation experiment, ~9 g surface sediment samples (2 cm from top) were collected from the columns and spiked with 4 mg L^{-1} $HgCl_2$ solutions, forming final $HgCl_2$ concentration to be around 1 mg L^{-1} in sediment slurries. After homogeneous mixing, the slurries were divided into two portions. One portion was stored at −20 °C, representing Hg level at t = 0. And the remaining was incubated in the dark at 25 °C for 48 hours,

representing Hg level at t = 48 h. Spiking and dividing sediment samples were performed in an anaerobic chamber (LAI-3, Longyue, China). Duplicate was employed for both treatments. Thus, for each treatment of the MPA mitigation experiment, there are four parallel samples for MPA analysis. In addition, a portion of surface sediment (without the addition of $HgCl_2$ solution) was stored at −80 ℃ for microbiological assay.

2) Physicochemical parameter analysis in the columns

Concentrations of DO in the overlying water and ORP at the sediment-water interface were analyzed at regular intervals. On the sampling days, concentrations of dissolved organic carbon (DOC) and sulfate (SO_4^{2-}) in the overlying water, as well as total carbon (C), total nitrogen (N), total sulfide (S), total organic carbon (TOC), and moisture content in surface sediment samples were analyzed respectively. Detailed analytical methods of these parameters can be found in the SI.

2.3 THg and MeHg analysis

For THg analysis in the sediment samples, a Hydra-C mercury analyzer (Teledyne Leeman Labs, USA) following US EPA method 7473 was adopted (USEPA, 2007). For THg analysis in the water samples, the MERX Automatic THg System (Brooks Rand Laboratories, USA) following US EPA method 1631 was adopted (USEPA, 2002). For MeHg analysis in the sediment samples, the pretreatment procedure using $CuSO_4/HNO_3$ as leaching solutions was applied (Ji et al., 2019). Then MeHg concentrations were determined with MERX Automatic Methylmercury System (Brooks Rand Laboratories, USA) following US EPA method 1630 (USEPA, 2001).

2.4 DNA extraction and Real-Time Quantitative PCR (qPCR)

Total microbial DNA was extracted from approximately 0.25 g freeze-dried surface sediment samples in the column experiment using DNeasy PowerSoil Kit (QIAGEN Inc., Germany) following the manufacturer's recommended protocol. Concentrations and quality of the extracted DNA were determined with a Nanodrop UV-Vis spectrophotometer (ND-2000, Thermo-Fisher Scientific, USA), and the abundance of the *hgcA* gene was quantified using an iCycler iQ5 thermocycler (Bio-Rad, USA). The clade-specific degenerate primer pair for Deltaproteobacteria was ORNL-Delta-HgcA (Delta-HgcA-F: GCCAACTACAAG MTGASCTWC; Delta-HgcA-R: CCSGCNGCRCACCAGACRTT) (Liu et al., 2018b).

2.5 Calculation of MeHg production ability (MPA)

The MPA of surface sediment from the columns was calculated according to the modified equation for Hg methylation rate calculation (**Eq. 1**) (Hintelmann et al., 2000).

$$\text{MeHg production ability} = \frac{[\text{MeHg}]_{48} - [\text{MeHg}]_0}{[\text{Hg}^{2+}]_0} \qquad \textbf{(Eq. 1)}$$

where $[MeHg]_{48}$ represented MeHg concentration 48 h after the addition of $HgCl_2$ solution, $[MeHg]_0$ represented MeHg concentration the instant after the addition of $HgCl_2$ solution. $[Hg^{2+}]_0$ represented Hg^{2+} concentration the instant after the addition of $HgCl_2$ solution, which could be achieved by subtracting the content of MeHg from THg.

2.6 Quality assurance/quality control (QA/QC) and statistical analysis

During MeHg analysis in the sediment, MeHg concentrations in the certified reference material ERM-CC580 (certified MeHg content: 75.5 ± 3.7 ng g^{-1}, European Reference

Materials, Institute for Reference Materials and Measurements, Belgium) were also analyzed, with the average value being 76.0 ± 7.2 ng g^{-1} (n = 3). The limit of quantification (LOQ) was 5 pg Hg in absolute mass, suggesting a good sensibility of the analytical method. Besides, the linear range is from 5 to 800 pg (r^2 = 0.99). For THg analysis in the sediment, GSD-10 (GBW07310, Institute of Geological and Geophysical Exploration, Chinese Academy of Geological Sciences, China) was used as certified reference material. The average THg concentration measured was 280.02 ± 0.06 ng g^{-1} (n=3), which agreed well with the certified value (280 ± 40 ng g^{-1}).

The differences between two groups throughout the incubation were analyzed using a paired-sample *t* test after the normality test, and differences on every sampling day were assessed by an independent *t* test. Significance probabilities (*p*) were also calculated and the difference was declared significantly for $p < 0.05$.

3. Results

3.1 Characteristics of overlying water and surface sediment

As shown in **Table 1**, the concentrations of TP, TN, and Chlorophyll *a* in the overlying water of Taihu Lake were 0.13 ± 0.01, 10.28 ± 0.29 mg L^{-1}, and 182.90 ± 10.79 μg L^{-1}. These were consistent with reported results and were typical characteristics of a hyper-eutrophic freshwater (Xu et al., 2017). The average THg concentration in surface sediment was 13.38 ± 0.31 ng g^{-1}, and the ratio of MeHg to THg was 11.96‰. In the overlying water, THg concentration was 1.2‰ of that in the surface sediment, and MeHg concentration was below detection limit. These results fell within the range typically measured in Taihu Lake

241 (Wang et al., 2012). In addition, the THg content in Taihu Lake's surface sediment was much
242 lower than $HgCl_2$ concentrations added in the Hg methylation experiment (approximately 0.1,
243 1, and 10 mg L^{-1} in the slurries), which indicated that the potential influence of the
244 background Hg was negligible.

Table 1. Physiochemical characteristics of the overlying water and surface sediment samples collected from Taihu Lake (data shown by mean ± SD, n = 2).

		Overlying water	Surface sediment
TP	mg L^{-1}	0.13 ± 0.01	-
PO_4^{3-}		0.04 ± 0.00	-
TN		10.28 ± 0.29	-
NO_3^-		0.51 ± 0.07	-
DOC		33.39 ± 0.30	-
Chlorophyll *a*	μg L^{-1}	182.90 ± 10.79	-
THg	ng L^{-1}	11.34 ± 1.35	13.38 ± 0.31
MeHg	(ng g^{-1})	ND	0.16 ± 0.02
C	%	-	0.40 ± 0.02
N		-	0.06 ± 0.00
S		-	0.05 ± 0.00
TOC		-	0.29 ± 0.01
Moisture content		-	63.90 ± 0.50
C/N	-	-	7.35 ± 0.32

Note: ND represented not detected. The unit of "ng L^{-1}" was for concentrations in the overlying water and "ng g^{-1}" was for sediments.

3.2 Hg fate in simulated Hg-polluted sediment-water system

The Hg methylation experiment was designed to verify MeHg production in the sediment in case abrupt Hg pollution occurs in eutrophic waters. Moreover, in order to investigate the effects of O_2 nanobubbles on MPA, MeHg production in the sediment after the addition of $HgCl_2$ solution should be sufficient for quantification. Therefore, the optimal dosage of $HgCl_2$ solution for MPA analysis was determined according to the Hg fate after the addition of three different concentrations of $HgCl_2$ solutions (10, 100, and 1000 mg L^{-1}) with the final concentrations being around 0.1, 1, and 10 mg L^{-1} in the slurries. **Fig. 2** illustrated the variations of MeHg and THg in the sediment (after the extraction of overlying water) after the addition of $HgCl_2$ solutions.

As illustrated in **Fig. 2A**, MeHg concentrations in the 10 mg L^{-1}, 100 mg L^{-1}, and 1000 mg L^{-1} groups all increased significantly since day 0, with the maximum increments being 47.6, 35.5, and 10.0 times, respectively. This demonstrated the spontaneous MeHg production in the sediment after the outbreak of Hg pollution in eutrophic waters. Particularly, all three groups experienced the most remarkable increase in MeHg concentrations from day 0 to 2 (by 18.9, 11.7, and 7.2 times, respectively), and then MeHg concentrations varied minimally till the end of the Hg methylation experiment. According to this, the incubation length of MPA analysis in the sediment was designed as 48 h (**Eq. 1**). Compared with MeHg, THg concentrations varied little over time (**Fig. 2B**). In addition, MeHg and THg concentrations in the overlying water were analyzed as well (SI, **Fig. S2**). We found that for each group, MeHg and THg concentrations in the sediment (1.28–724.56 and 475.09–30864.36 ng g^{-1}) were generally three orders of magnitude higher than those in the overlying

water (0–1013.18 and 15.93–1776.46 ng L^{-1}) throughout the experiment. These results indicated that sediment was the main sink of Hg in surface waters.

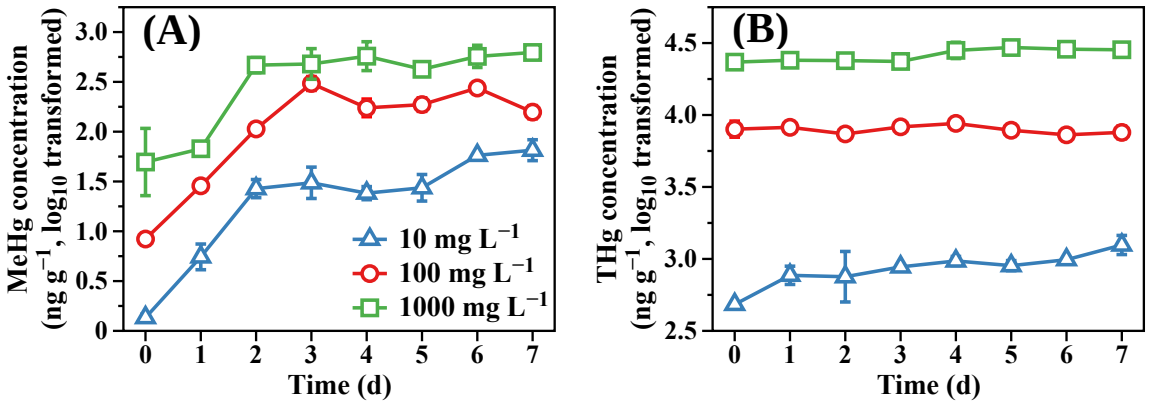

Fig. 2. Variations of (A) MeHg and (B) THg concentrations in the sediment during the 7-day Hg methylation experiment. All data was transformed to log_{10} form, and the mean and standard deviation (SD) were calculated accordingly. Day 0 represented Hg level the instant after the addition of $HgCl_2$ solution. Figure legend (i.e.10 mg L^{-1}, 100 mg L^{-1}, 1000 mg L^{-1}) referred to the concentrations of the spiking $HgCl_2$ solution (data shown by mean ± SD, n = 2).

Moreover, with different dosages of $HgCl_2$ solutions, the MeHg fates in the sediment were significantly ($p < 0.001$) different (**Fig. 2A**). Among the three groups, the 10 mg L^{-1} group produced the fewest MeHg in the sediment, from 1.36 ng g^{-1} (day 0) to 27.07 ng g^{-1} (day 2) and 66.07 ng g^{-1} (day 7). While in the 100 mg L^{-1} and 1000 mg L^{-1} groups, MeHg concentrations increased maximally from 8.38 to 306.19 ng g^{-1} (day 0 to 3) and 57.18 to 626.35 ng g^{-1} (day 0 to 7), respectively. Specifically, the average MeHg concentrations in the two groups on day 2 were 106.57 and 468.91 ng g^{-1}, far exceeding that in the 10 mg L^{-1} group. This suggested that 10 mg L^{-1} (the added $HgCl_2$ concentration) might not be the

optimal Hg dosage for MPA analysis due to its low MeHg production. In addition, differences in MeHg concentrations between the 100 mg L^{-1} and 1000 mg L^{-1} groups (3.4 times on day 2) were smaller than the difference in the adding concentrations (10 times). This suggested that 100 mg L^{-1} $HgCl_2$ solution might produce higher MeHg production in the sediment and was most suitable for the MPA mitigation experiment. In addition, the average THg concentration in the sediment (from day 1 to 7) of the 10 mg L^{-1} group (852.46 ng g^{-1}) was approximately 1/9 of the 100 mg L^{-1} group (7519.36 ng g^{-1}) and 1/28 of the 1000 mg L^{-1} group (23686.35 ng g^{-1}) (**Fig. 2B**), which might be related to the adsorption capacity of Hg on the sediment (Ikingura and Akagi, 1999).

In general, there would be spontaneous MeHg production in the Hg-polluted eutrophic waters, and the sediment was the major Hg sink in the system. Moreover, the MPA in the sediment would be analyzed with the production of MeHg within 48 h after the addition of 1 mg L^{-1} $HgCl_2$ in the sediment-water slurry.

3.3 Variations of MPAs in the surface sediment

Considering that surface sediment in aquatic system has been reported to be the hot spot for Hg methylation (Ullrich et al., 2001), the differences in MPA of surface sediment between the Control and O_2 NBs groups throughout the 20-d incubation period were analyzed and illustrated in **Fig. 3**. The two groups were designed to examine the mitigation effects of interfacial O_2 nanobubbles on the MPA of surface sediment (**Fig. 1B**). Generally, the MPAs in the O_2 NBs group (2.8–12.5‰) were lower than those in the Control group (4.7–15.5‰), particularly from the medium term of the incubation. During the first four days, there was no significant difference in the MPA between the two groups. However, from day 8 to 20, the

MPA in the O_2 NBs group decreased significantly compared to the Control group, with the decrements being 45%, 40%, and 48% on days 8, 12, and 20 ($p < 0.01$, 0.05, and 0.05), respectively. Moreover, in the Control group, the MPA reached its peak of 14.3 ± 1.2‰ on day 12. This indicated that massive MeHg production in surface sediment would appear around 12 days after the outbreak of Hg pollution in the eutrophic waters, and that requires particular concern. While in the O_2 NBs group, the peak of MPA (10.4 ± 0.4‰) appeared on day 4 and decreased significantly ($p < 0.05$ on day 8 and $p < 0.01$ on day 20) hereafter.

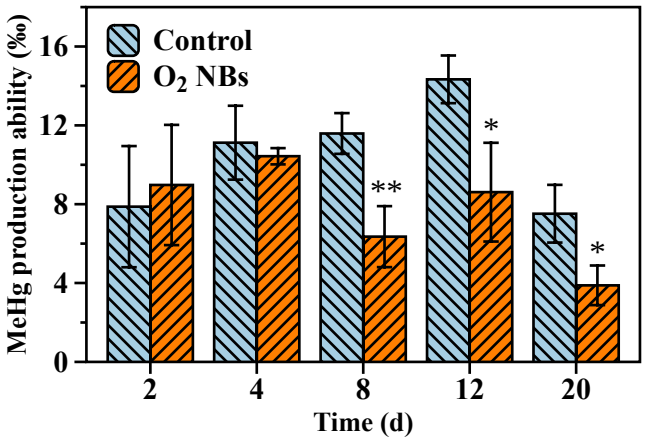

Fig. 3. Comparison of MeHg production ability of surface sediment from columns with (O_2 NBs) and without (Control) O_2 nanobubbles during the 20-day experiment. The column experiments and Hg methylation experiments were both performed in duplicate, and the data was shown by mean ± SD, n = 4. "*" indicates that the significant difference in average MPA between the Control and O_2 NBs groups is $p < 0.05$; "**" indicates the significant difference is $p < 0.01$.

As MeHg production in surface sediment was mainly microbially mediated (Yu et al., 2012), the variations of environmental factors related to the Hg microbial methylator activities, such as redox conditions and organic matter, might contribute to the reduction

effects on MPA by O_2 nanobubbles. Therefore, variations of such factors were analyzed and illustrated in the overlying water (**Fig. 4**) and surface sediment (**Fig. 5**) from the two groups.

3.3.1 Variations of DO, ORP, SO_4^{2-}, and DOC in the overlying water

As illustrated in **Fig. 4**, concentrations of DO, ORP, SO_4^{2-}, and DOC in the overlying water between the two groups were significantly different during the 20-d incubation period.

Among these factors, DO, ORP, and SO_4^{2-} have been suggested to illustrate the redox conditions in the overlying water (Duvil et al., 2018; Zhang et al., 2018). First of all, as shown in **Fig. 4A**, the DO concentrations in the overlying water from the O_2 NBs group were significantly higher than those in the Control group throughout the incubation ($p < 0.01$). Specifically, the DO concentrations in both groups began from 0 on day −1, and those in the Control group maintained the level till day 20. However, after the addition of O_2 nanobubbles on day 0, DO concentrations in the O_2 NBs group displayed a sudden increase and reached up to 2.1 mg L^{-1}. Even though the DO concentrations in the O_2 NBs group then decreased from day 1, the significant elevation ($p < 0.01$) from the Control group remained until day 8.

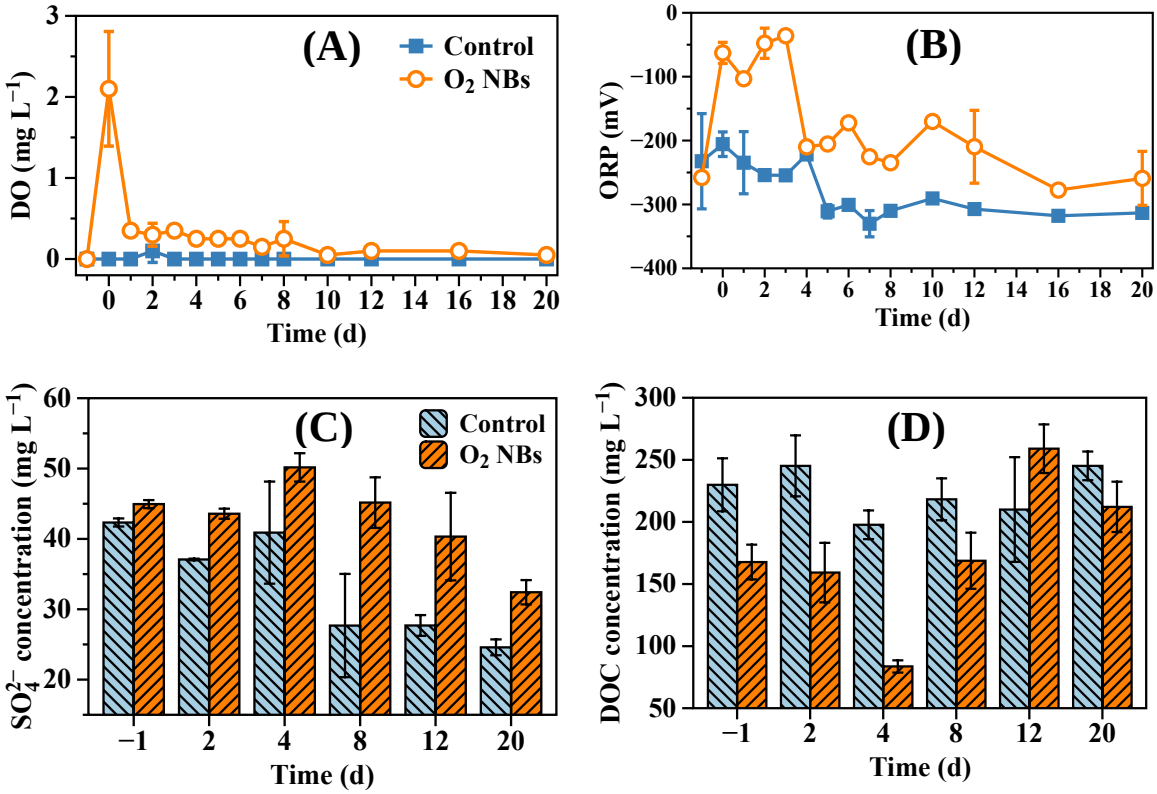

340 **Fig. 4.** Concentrations of (A) DO; (B) ORP; (C) SO_4^{2-}; and (D) DOC in the overlying water
341 from columns with (O_2 NBs) and without (Control) O_2 nanobubbles. Day −1 represented the
342 content before the addition of O_2 nanobubbles. The column experiments were performed in
343 duplicate and the data was shown by mean ± SD, n = 2.

344 The variations of ORP at the sediment-water interface from both groups are illustrated
345 in **Fig. 4B**. Throughout the incubation period, the ORP in the Control group was in the range
346 of −344.7 to −192.0 mV, with the average being −280.9 mV, which might reveal the anoxia
347 caused by the decomposition of the dead algae. However, the addition of O_2 nanobubbles
348 significantly ($p < 0.001$) increased the ORP throughout the incubation (in the range of −289.1
349 to −30.5 mV). From day −1 to day 0, the average ORP in the O_2 NBs group was elevated
350 from −257.9 to −62.8 mV, by a ratio of 76%. The ORP in the O_2 NBs group was significantly

higher than that in the Control group from day 0 to 3, with the differences being 69%, 56%, 81%, and 86% on each day. From then on to day 20, the gap between the two groups narrowed, but the ORP in the O_2 NBs group was still beyond the Control group.

Fig. 4C illustrates the comparison result of SO_4^{2-} concentrations in the overlying water between the Control and O_2 NBs groups. The average SO_4^{2-} concentration in all the columns on day −1 was 49.64 ± 6.42 mg L^{-1}. Since the beginning of the experiment, the SO_4^{2-} concentrations in the O_2 NBs group (31.20–51.59 mg L^{-1}) were significantly ($p < 0.001$) elevated from to the Control group (22.50–46.03 mg L^{-1}), with the maximum increment being 63% on day 8. The increase of SO_4^{2-} concentrations in the O_2 NBs group corresponded with the increase of DO and ORP content, and all could reveal the enhanced oxidative condition in the columns.

Moreover, as shown in **Fig. 4D**, the variation of DOC concentrations in the overlying water after the addition of O_2 nanobubbles was the opposite of DO, ORP, and SO_4^{2-}. In general, the DOC concentrations in the O_2 NBs group were significantly lower than the Control group ($p < 0.05$). Compared with the content in Taihu Lake water (33.39 ± 0.30 mg L^{-1}, **Table 1**), the DOC concentrations in the Control and O_2 NBs groups increased significantly on day −1, to 229.88 and 167.70 mg L^{-1} (by 5.9 and 4.0 times), respectively. On days 2 and 4, the DOC concentrations in the O_2 NBs group decreased significantly ($p < 0.01$) compared with the Control group, with the decrements being 35% and 58% respectively. As the DOC content could represent the content of dissolved organic matter (DOM), the decrease in the DOC concentrations in the O_2 NBs group could indicate a reduction of DOM in the overlying water.

3.3.2 Variations of S, TOC, and ratio of C and N (C/N) in the surface sediment

The variations of factors in the surface sediment were likely to bring direct influences on MPA. Thus, relative factors affecting MeHg production, including redox conditions and organic matter content in surface sediment, were analyzed as well. The content of S, TOC, and ratios of C and N (C/N) in the surface sediment is illustrated in **Fig. 5**.

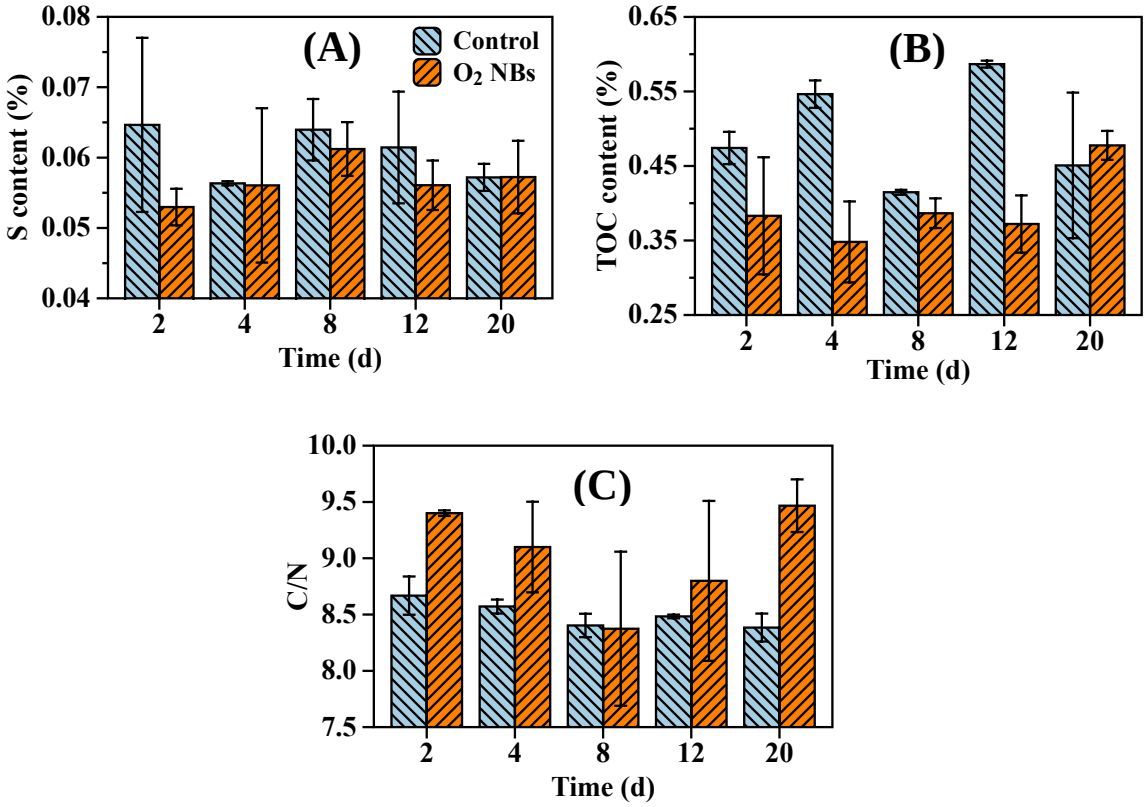

Fig. 5. Comparison of (A) S content, (B) TOC content, and (C) ratio of C and N content in the surface sediment from columns with (O_2 NBs) and without (Control) O_2 nanobubbles. The column experiments were performed in duplicate and the data was shown by mean ± SD, n = 2.

Sulfur content has been suggested to reflect the redox conditions in the sediment and might be influenced by changes in the valence of sulfide and activities of sulfate-reducing

bacteria there (Zhu et al., 2017; Gilmour et al., 2011). Accordingly, the S content in the surface sediment from the Control and O_2 NBs groups was analyzed throughout the incubation period. As illustrated in **Fig. 5A**, the S content in both groups varied slightly during the incubation and was similar with the content in the Taihu Lake sediment (**Table 1**). Compared with that in the Control group, the S content in the O_2 NBs group was generally lower, with the largest difference being 18% on day 2. These results might partially suggest the oxidation by O_2 nanobubbles on surface sediment.

In addition, the TOC content could reflect the content of organic matter in surface sediment. As shown in **Fig. 5B**, the TOC concentrations in the O_2 NBs group were significantly lower than the Control group during the incubation ($p < 0.05$). The decrement between the two groups reached its peak by 37% on day 12 (59% and 37% in the Control and O_2 NBs groups, respectively). The TOC content in the surface sediment from the Control group reached its maximum on day 12, well consistent with the variation of MPA. Moreover, the ratio of C and N content could reflect the origin and decomposition of organic matter in the sediment. Compared with the Control group, O_2 nanobubbles significantly increased the ratios of C/N in the surface sediment during the incubation ($p < 0.001$). By comparing the C and N content in the two groups (**Fig. S3**), we discovered that the N content in the O_2 NBs group was generally lower than the Control group from day 2 to 12 with an average decrease by 9.2%. On days 12 and 20, C content in the O_2 NBs group increased by 2.6% and 26.7% on either day.

To sum up, after the addition of interfacial O_2 nanobubbles, the MPA of surface sediment decreased significantly during the incubation period. Meanwhile, in the overlying

water, O_2 nanobubbles led to the elevation of DO, ORP, and SO_4^{2-} and the decline of DOC. In the surface sediment, the content of S and TOC decreased significantly after the addition of O_2 nanobubbles while the C/N ratios increased conversely. Variations of these factors could contribute to the reduction of MPA, as will be discussed later.

3.4 *hgcA* abundances in the surface sediment

The *hgcA* gene was reported to indicate the abundances of Hg microbial methylators (Liu et al., 2018b). The variations of *hgcA* abundances might help explain the reduction of MPA after the addition of O_2 nanobubbles from the perspective of microbiology. Accordingly, in the MPA mitigation experiment, abundances of *hgcA* gene in the surface sediment from the Control and O_2 NBs groups were analyzed and illustrated in **Fig. 6**.

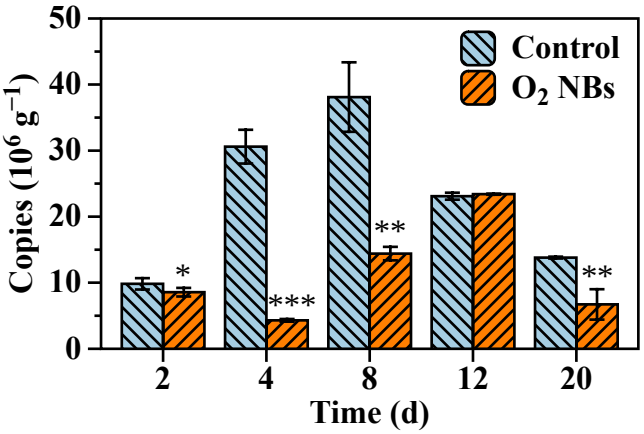

Fig. 6. Variation of *hgcA* gene abundance in the surface sediment from columns with (O_2 NBs) and without (Control) O_2 nanobubbles. The symbol of "*" represented $p < 0.05$, "**" represented $p < 0.01$, and "***" represented $p < 0.001$.

As shown in the figure, the *hgcA* abundances decreased significantly after the addition of O_2 nanobubbles ($p < 0.01$). In the Control and O_2 NBs groups, the *hgcA* abundances were

in the range of 9.23–42.67 and 7.04–23.41 × 10^6 copies g^{-1}, respectively. The largest decrease between the two groups was 86% on day 4, from 30.60 × 10^6 to 4.30 × 10^6 copies g^{-1}. Specifically, abundance of *hgcA* in the surface sediment from the Control group reached its peak at 3.81 ×10^7 copies g^{-1} on day 8. The peak appeared slightly ahead of the peak of MPA on day 12 in the Control group (**Fig. 2**). While in the O_2 NBs group, the *hgcA* abundance reached its maximum (23.40 × 10^6 copies g^{-1}) on day 12. The decline in the O_2 NBs group suggested that O_2 nanobubbles might be capable of reducing Hg microbial methylator densities in the surface sediment of eutrophic waters, and the potential causes of the decline will be discussed later.

4. Discussion

4.1 Hg sink and source in the aquatic system

In the Hg methylation experiment, the THg content in the sediment (**Fig. 2B**) was significantly higher than that in the overlying water (**Fig. S2B**), which is consistent with reported results (Wang et al., 2009). The huge difference (over three orders of magnitude) between the sediment and overlying water implied that sediment could be the major Hg sink if there is abrupt Hg pollution in the surface waters. It has been reported that once introduced to aquatic ecosystem, Hg is primarily complexed with dissolved organic matter and then diffused to the sediment layer, where the complexes might react with sulfide and form β-HgS nanoparticles (Slowey, 2010). Moreover, the effective binding of Hg and particles in sediment might restrain the migration of Hg into overlying water (Stein et al., 1996). This could help explain the difference in THg content between the sediment and overlying water

in this work. Indeed, high THg content (up to 2010 μg g^{-1}) has also been observed in the sediment after massive Hg-polluted effluent was discharged in Minamata Bay from 1932 to 1968. In addition, the retention time of Hg in sediment was reported to be quite long. At the time of the dredging operation in 1990, Hg content in the sediment was still as high as 25 μg g^{-1} (Hachiya, 2012).

Apart from that, due to hydraulic exchanging at the sediment-water interface, Hg could also be released into overlying water, which made sediment an important Hg source as well (Hester et al., 2009). MeHg has been reported to be the main Hg species entering overlying water from sediments in a bay impacted by Hg discharges (Gill et al., 1999). Considering the much higher content of THg and organic matter in sediment, MeHg production is predominant in the sediment rather than in the overlying water (Qiu et al., 2005; Compeau and Bartha, 1985). Subsequently, MeHg might enter food web via pore water but without substantial photodegradation in deep water (Balogh et al., 2015). In particular, for shallow lakes, the sediment-water exchange has been suggested to remarkably influence the distribution of Hg and MeHg in the overlying water (Choe et al., 2004). Therefore, even though sediment could take up a majority of exogenous Hg once Hg-polluted wastewater was discharged, it could still release a fair amount of MeHg into the overlying water and cause adverse effects on it.

4.2 Effects of interfacial oxygen nanobubbles

In the MPA mitigation experiment, the MPA of surface sediment decreased significantly after the addition of O_2 nanobubbles, as shown in **Fig. 3**. This agreed well with the reported results that MeHg content in sediment was lower under aerobic (bubbled with air) than in

anaerobic conditions (bubbled with nitrogen) (Duvil et al., 2018). Hg methylation in natural waters has been reported to be predominantly mediated by microorganisms (Jiang et al., 2018). Therefore, the variations of Hg microbial methylators could largely explain the variations of MPA. The addition of O_2 nanobubbles might induce fluctuations of relative factors in the overlying water and surface sediment. This would trigger changes in activities of Hg microbial methylators, which may be illustrated by the variation of *hgcA* abundances. As a result, the MPA of surface sediment would vary after the addition of O_2 nanobubbles. This might help explain the positive correlation between MPA and *hgcA* abundance (SI, **Fig. S4A**). Moreover, different environmental factors might induce different effects on Hg microbial methylator activities. Relative factors in the sediment-water columns could be divided into two categories, one was factors regarding redox conditions, and the other was relative to organic matter.

4.2.1 Enhancement of oxidative conditions

The content of DO, ORP, and SO_4^{2-} in the overlying water and S in surface sediment could reflect the variation of redox conditions in the sediment-water columns. Apart from the obviously elevated DO and ORP after the addition of O_2 nanobubbles, the SO_4^{2-} concentrations in the overlying water were significantly increased as well. In addition, sulfides (such as FeS and FeS_2) in the sediment might be oxidized to SO_4^{2-}, which was likely to enter overlying water (Zhu et al., 2017; Schippers and Jørgensen, 2002). To some extent, the decrease in S content in the O_2 NBs group might reveal the oxidation process in the surface sediment by O_2 nanobubbles. In addition, the *hgcA* abundance was found to be negatively correlated with DO, ORP, and SO_4^{2-} and positively correlated with S (SI, **Fig.**

S4B–E). It has been reported that aerobic conditions may inhibit the growth of Hg microbial methylators, and that biotic Hg methylation mainly occurs in the anaerobic conditions (Regnell and Tunlid, 1991). Take sulfate-reducing bacteria for instance, high content of DO (over 1 mg L^{-1}) and ORP (over −100 mV) has been proved to reduce the growth of them (Hao et al., 1996). Accordingly, the significantly elevated content of DO and ORP in the O_2 NBs group was suggested to inhibit the growth of sulfate-reducing bacteria, which might limit their abilities to produce MeHg. Apart from that, Hg methylation was reported to be accompanied by the reduction of SO_4^{2-} by sulfate-reducing bacteria (Yu et al., 2012). Therefore, the increase of SO_4^{2-} concentrations in the overlying water and decrease of S content in the surface sediment might also reveal the reduction of sulfate-reducing bacteria's activities after the addition of O_2 nanobubbles.

4.2.2. Reduction of organic matter

Another important factor that could regulate MeHg production is organic matter. The concentrations of DOC in the overlying water and TOC in surface sediment both decreased significantly after the addition of O_2 nanobubbles. In addition, there was an increase in the ratios of C/N in the surface sediment of the O_2 NBs group.

It has been proposed that organic matter can facilitate Hg methylation by manipulating activities of Hg microbial methylators (Drott et al., 2007). In this study, the decrease of DOC and TOC content after the addition of O_2 nanobubbles might indicate a reduction of organic matter. In particular, organic matter with lower C/N, usually originated from fresh chlorophyll, has been suggested to be highly labile to Hg microbial methylators (Bravo et al., 2017). The C/N ratio in the O_2 NBs group was comparatively higher than that in the Control

group, which suggested the decrease of labile organic matter. The decrease of labile organic matter might be related to the enhanced mineralization in the oxidative condition (Olson and Barbier, 1994), which could be induced by O_2 nanobubbles. In addition, in this study, interfacial O_2 nanobubbles were loaded on natural zeolite, which is a common capping material in surface waters. By blocking pollutants from entering the overlying water, O_2 nanobubble-loaded zeolites were capable of reducing microbial substrates like organic matter from entering the overlying water; this could also contribute to the decrease of DOC concentrations in the overlying water. These results might help explain the correlations between *hgcA* and DOC, TOC, and C/N (SI, **Fig. S4F-H**).

As a result, O_2 nanobubbles could lead to the enhanced oxidative condition and reduction of labile organic matter, and contribute to the inhibition of Hg microbial methylators. This could in turn lead to the decrease of MeHg production abilities in the surface sediment.

Still it is likely that MPA analysis using the surface sediment sampled from the columns might not perfectly reflect *in situ* MeHg production. But since Hg methylation was reported to be mainly mediated by microorganisms, and variations of factors in the overlying water and surface sediment might affect microbial activities, MeHg production abilities could therefore be altered.

5. Conclusions

In this work, eutrophic waters were demonstrated to be able to spontaneously produce MeHg if severe Hg pollution occurs, and Hg were mainly buried in the sediment. The

technology of interfacial oxygen nanobubbles proved to significantly reduce MeHg production abilities of the surface sediment. The alleviation of anoxia and reduction of organic matter induced by O_2 nanobubbles could contribute to the decrease of MPA. Moreover, the abundance of Hg microbial methylators was suggested to decrease significantly after the addition of O_2 nanobubbles. Considering the potentially enhanced MeHg production at the surface sediment of eutrophic waters due to the serious hypoxia/anoxia and organic matter accumulation, this study proposed a promising strategy for MeHg production ability remediation in case Hg pollution occurs.

Acknowledgement

This work was financially supported by the National Key R&D Program of China (2017YFA0207204).

References

Balogh, S. J., Tsui, M. T.-K., Blum, J. D., Matsuyama, A., Woerndle, G. E., Yano, S., Tada, A., 2015. Tracking the fate of mercury in the fish and bottom sediments of Minamata Bay, Japan, using stable mercury isotopes. Environ. Sci. Technol. 49, 5399-5406.

Bravo, A. G., Bouchet, S., Tolu, J., Björn, E., Mateos-Rivera, A., Bertilsson, S., 2017. Molecular composition of organic matter controls methylmercury formation in boreal lakes. Nat. Commun. 8, 14255.

Choe, K.-Y., Gill, G. A., Lehman, R. D., Han, S., Heim, W. A., Coale, K. H., 2004. Sediment-water exchange of total mercury and monomethyl mercury in the San Francisco Bay-Delta. Limnol. Oceanogr. 49, 1512-1527.

551 Compeau, G., Bartha, R., 1985. Sulfate-reducing bacteria: principal methylators of mercury
552 in anoxic estuarine sediment. Appl. Environ. Microbiol. 50, 498-502.
553 Conley, D. J., Paerl, H. W., Howarth, R. W., Boesch, D. F., Seitzinger, S. P., Havens, K. E.,
554 Lancelot, C., Likens, G. E., 2009. Controlling eutrophication: nitrogen and
555 phosphorus. Science. 323, 1014-1015.
556 Drott, A., Lambertsson, L., Björn, E., Skyllberg, U., 2007. Do potential methylation rates
557 reflect accumulated methyl mercury in contaminated sediments? Environ. Sci.
558 Technol. 42, 153-158.
559 Duvil, R., Beutel, M. W., Fuhrmann, B., Seelos, M., 2018. Effect of oxygen, nitrate and
560 aluminum addition on methylmercury efflux from mine-impacted reservoir sediment.
561 Water Res. 144, 740-751.
562 Feng, X., Dai, Q., Qiu, G., Li, G., He, L., Wang, D., 2006. Gold mining related mercury
563 contamination in Tongguan, Shaanxi Province, PR China. Appl. Geochem. 21, 1955-
564 1968.
565 Feng, Z., Fan, C., Huang, W., Ding, S., 2014. Microorganisms and typical organic matter
566 responsible for lacustrine "black bloom". Sci. Total Environ. 470-471, 1-8.
567 Gill, G. A., Bloom, N. S., Cappellino, S., Driscoll, C. T., Dobbs, C., McShea, L., Mason, R.,
568 Rudd, J. W., 1999. Sediment-water fluxes of mercury in Lavaca Bay, Texas. Environ.
569 Sci. Technol. 33, 663-669.
570 Gilmour, C., Bell, T., Soren, A., Riedel, G., Riedel, G., Kopec, D., Bodaly, D., Ghosh, U.,
571 2018. Activated carbon thin-layer placement as an in situ mercury remediation tool
572 in a Penobscot River salt marsh. Sci. Total Environ. 621, 839-848.

573 Gilmour, C. C., Elias, D. A., Kucken, A. M., Brown, S. D., Palumbo, A. V., Schadt, C. W.,
574 Wall, J. D., 2011. Sulfate-reducing bacterium *Desulfovibrio desulfuricans* ND132 as
575 a model for understanding bacterial mercury methylation. Appl. Environ. Microbiol.
576 77, 3938-3951.
577 Gilmour, C. C., Riedel, G. S., Riedel, G., Kwon, S., Landis, R., Brown, S. S., Menzie, C. A.,
578 Ghosh, U., 2013. Activated carbon mitigates mercury and methylmercury
579 bioavailability in contaminated sediments. Environ. Sci. Technol. 47, 13001-13010.
580 Gobeil, C., Macdonald, R. W., Smith, J. N., 1999. Mercury profiles in sediments of the Arctic
581 Ocean basins. Environ. Sci. Technol. 33, 4194-4198.
582 Gu, B., Bian, Y., Miller, C. L., Dong, W., Jiang, X., Liang, L., 2011. Mercury reduction and
583 complexation by natural organic matter in anoxic environments. Proc. Natl. Acad.
584 Sci. 108, 1479-1483.
585 Hachiya, N., Epidemiological update of methylmercury and Minamata disease. Reference to
586 a book: Methylmercury and neurotoxicity. Springer. 2012, pp. 1-11.
587 Hao, O. J., Chen, J. M., Huang, L., Buglass, R. L., 1996. Sulfate-reducing bacteria. Crit. Rev.
588 Env. Sci. Tec. 26, 155-187.
589 Harris, R. C., Rudd, J. W., Amyot, M., Babiarz, C. L., Beaty, K. G., Blanchfield, P. J.,
590 Bodaly, R., Branfireun, B. A., Gilmour, C. C., Graydon, J. A., 2007. Whole-
591 ecosystem study shows rapid fish-mercury response to changes in mercury
592 deposition. Proc. Natl. Acad. Sci. 104, 16586-16591.
593 Hester, E. T., Doyle, M. W., Poole, G. C., 2009. The influence of in-stream structures on
594 summer water temperatures via induced hyporheic exchange. Limnol. Oceanogr. 54,
595 355-367.

596 Hintelmann, H., Keppel-Jones, K., Evans, R. D., 2000. Constants of mercury methylation
597 and demethylation rates in sediments and comparison of tracer and ambient mercury
598 availability. Environ. Toxicol. Chem. 19, 2204-2211.
599 Huisman, J., Codd, G. A., Paerl, H. W., Ibelings, B. W., Verspagen, J. M. H., Visser, P. M.,
600 2018. Cyanobacterial blooms. Nat. Rev. Microbiol. 16, 471-483.
601 Ikingura, J. R., Akagi, H., 1999. Methylmercury production and distribution in aquatic
602 systems. Sci. Total Environ. 234, 109-118.
603 Ji, X., Liu, C., Shi, J., Pan, G., 2019. Optimization of pretreatment procedure for MeHg
604 determination in sediments and its applications. Environ. Sci. Pollut. R. 26, 17707-
605 17718.
606 Jiang, G.-B., Shi, J.-B., Feng, X.-B., 2006. Mercury pollution in China. Environ. Sci.
607 Technol. 40, 3672-3678.
608 Jiang, T., Bravo, A. G., Skyllberg, U., Björn, E., Wang, D., Yan, H., Green, N. W., 2018.
609 Influence of dissolved organic matter (DOM) characteristics on dissolved mercury
610 (Hg) species composition in sediment porewater of lakes from southwest China.
611 Water Res. 146, 148-158.
612 Krabbenhoft, D. P., Sunderland, E. M., 2013. Global change and mercury. Science. 341,
613 1457-1458.
614 Lamborg, C. H., Hammerschmidt, C. R., Bowman, K. L., Swarr, G. J., Munson, K. M.,
615 Ohnemus, D. C., Lam, P. J., Heimbürger, L.-E., Rijkenberg, M. J., Saito, M. A., 2014.
616 A global ocean inventory of anthropogenic mercury based on water column
617 measurements. Nature. 512, 65-68.

618 Lei, P., Nunes, L. M., Liu, Y.-R., Zhong, H., Pan, K., 2019. Mechanisms of algal biomass
619 input enhanced microbial Hg methylation in lake sediments. Environ. Int. 126, 279-
620 288.
621 Li, P., Feng, X., Qiu, G., Shang, L., Li, Z., 2009. Mercury pollution in Asia: a review of the
622 contaminated sites. J. Hazard. Mater. 168, 591-601.
623 Li, Y., Yin, Y., Liu, G., Tachiev, G., Roelant, D., Jiang, G., Cai, Y., 2012. Estimation of the
624 major source and sink of methylmercury in the Florida Everglades. Environ. Sci.
625 Technol. 46, 5885-5893.
626 Liu, P., Ptacek, C. J., Blowes, D. W., Finfrock, Y. Z., Gordon, R. A., 2017. Stabilization of
627 mercury in sediment by using biochars under reducing conditions. J. Hazard. Mater.
628 325, 120-128.
629 Liu, P., Ptacek, C. J., Blowes, D. W., Gould, W. D., 2018a. Control of mercury and
630 methylmercury in contaminated sediments using biochars: A long-term microcosm
631 study. Appl. Geochem. 92, 30-44.
632 Liu, Y.-R., Johs, A., Bi, L., Lu, X., Hu, H.-W., Sun, D., He, J.-Z., Gu, B., 2018b. Unraveling
633 microbial communities associated with methylmercury production in paddy soils.
634 Environ. Sci. Technol. 52, 13110-13118.
635 Lyu, T., Wu, S., Mortimer, R. J. G., Pan, G., 2019. Nanobubble technology in environmental
636 engineering: revolutionization potential and challenges. Environ. Sci. Technol. 53,
637 7175-7176.
638 Mailman, M., Stepnuk, L., Cicek, N., Bodaly, R. A., 2006. Strategies to lower methyl
639 mercury concentrations in hydroelectric reservoirs and lakes: a review. Sci. Total
640 Environ. 368, 224-235.

641 Mason, R. P., 2013. Trace metals in aquatic systems. John Wiley & Sons.
642 Olson, T. M., Barbier, P. F., 1994. Oxidation kinetics of natural organic matter by sonolysis
643 and ozone. Water Res. 28, 1383-1391.
644 Parks, J. M., Johs, A., Podar, M., Bridou, R., Hurt, R. A., Smith, S. D., Tomanicek, S. J.,
645 Qian, Y., Brown, S. D., Brandt, C. C., 2013. The genetic basis for bacterial mercury
646 methylation. Science. 339, 1332-1335.
647 Podar, M., Gilmour, C. C., Brandt, C. C., Soren, A., Brown, S. D., Crable, B. R., Palumbo,
648 A. V., Somenahally, A. C., Elias, D. A., 2015. Global prevalence and distribution of
649 genes and microorganisms involved in mercury methylation. Sci. Adv. 1, e1500675.
650 Qiu, G., Feng, X., Wang, S., Shang, L., 2005. Mercury and methylmercury in riparian soil,
651 sediments, mine-waste calcines, and moss from abandoned Hg mines in east Guizhou
652 province, southwestern China. Appl. Geochem. 20, 627-638.
653 Regnell, O., Tunlid, A., 1991. Laboratory study of chemical speciation of mercury in lake
654 sediment and water under aerobic and anaerobic conditions. Appl. Environ.
655 Microbiol. 57, 789-795.
656 Schippers, A., Jørgensen, B. B., 2002. Biogeochemistry of pyrite and iron sulfide oxidation
657 in marine sediments. Geochim. Cosmochim. Acta. 66, 85-92.
658 Seddon, J. R., Lohse, D., Ducker, W. A., Craig, V. S., 2012. A deliberation on nanobubbles
659 at surfaces and in bulk. ChemPhysChem. 13, 2179-2187.
660 Shen, P. P., Shi, Q., Hua, Z. C., Kong, F. X., Wang, Z. G., Zhuang, S. X., Chen, D. C., 2003.
661 Analysis of microcystins in cyanobacteria blooms and surface water samples from
662 Meiliang Bay, Taihu Lake, China. Environ. Int. 29, 641-647.

663 Shi, W., Pan, G., Chen, Q., Song, L., Zhu, L., Ji, X., 2018. Hypoxia remediation and methane
664 emission manipulation using surface oxygen nanobubbles. Environ. Sci. Technol. 52,
665 8712-8717.
666 Slowey, A. J., 2010. Rate of formation and dissolution of mercury sulfide nanoparticles: The
667 dual role of natural organic matter. Geochim. Cosmochim. Acta. 74, 4693-4708.
668 Soerensen, A. L., Schartup, A. T., Gustafsson, E., Gustafsson, B. G., Undeman, E., Björn,
669 E., 2016. Eutrophication increases phytoplankton methylmercury concentrations in a
670 coastal sea—a Baltic Sea case study. Environ. Sci. Technol. 50, 11787-11796.
671 Stein, E. D., Cohen, Y., Winer, A. M., 1996. Environmental distribution and transformation
672 of mercury compounds. Crit. Rev. Env. Sci. Tec. 26, 1-43.
673 Streets, D. G., Devane, M. K., Lu, Z., Bond, T. C., Sunderland, E. M., Jacob, D. J., 2011.
674 All-time releases of mercury to the atmosphere from human activities. Environ. Sci.
675 Technol. 45, 10485-10491.
676 Sunderland, E. M., Krabbenhoft, D. P., Moreau, J. W., Strode, S. A., Landing, W. M., 2009.
677 Mercury sources, distribution, and bioavailability in the North Pacific Ocean: Insights
678 from data and models. Global Biogeochem. Cy. 23, GB2010.
679 Taranu, Z. E., Gregory-Eaves, I., Leavitt, P. R., Bunting, L., Buchaca, T., Catalan, J.,
680 Domaizon, I., Guilizzoni, P., Lami, A., McGowan, S., Moorhouse, H., Morabito, G.,
681 Pick, F. R., Stevenson, M. A., Thompson, P. L., Vinebrooke, R. D., 2015.
682 Acceleration of cyanobacterial dominance in north temperate-subarctic lakes during
683 the Anthropocene. Ecol Lett. 18, 375-384.

Ullrich, S. M., Tanton, T. W., Abdrashitova, S. A., 2001. Mercury in the aquatic environment: a review of factors affecting methylation. Crit. Rev. Env. Sci. Tec. 31, 241-293.

USEPA, Method 1630: Methyl Mercury in Water by Distillation, Aqueous Ethylation, Purge and Trap, and Cold Vapor Atomic Fluorescence Spectrometry, 2001.

USEPA, Method 1631: Mercury in Water by Oxidation, Purge and Trap, and Cold Vapor Atomic Fluorescence Spectrometry. Revision E, 2002.

USEPA, Method 7473: Mercury in Solids and Solutions by Thermal Decomposition, Amalgamation, and Atomic Absorption Spectrophotometry. 2007.

Wang, H., Dai, M., Liu, J., Kao, S.-J., Zhang, C., Cai, W.-J., Wang, G., Qian, W., Zhao, M., Sun, Z., 2016a. Eutrophication-driven hypoxia in the East China Sea off the Changjiang Estuary. Environ. Sci. Technol. 50, 2255-2263.

Wang, L., Miao, X., Ali, J., Lyu, T., Pan, G., 2018. Quantification of oxygen nanobubbles in particulate matters and potential applications in remediation of anaerobic environment. ACS Omega. 2018, 10624-10630.

Wang, L., Pan, G., Shi, W., Wang, Z., Zhang, H., 2016b. Manipulating nutrient limitation using modified local soils: A case study at Lake Taihu (China). Water Res. 101, 25-35.

Wang, S., Xing, D., Jia, Y., Li, B., Wang, K., 2012. The distribution of total mercury and methyl mercury in a shallow hypereutrophic lake (Lake Taihu) in two seasons. Appl. Geochem. 27, 343-351.

Wang, S., Jia, Y., Wang, S., Wang, X., Wang, H., Zhao, Z., Liu, B., 2009. Total mercury and monomethylmercury in water, sediments, and hydrophytes from the rivers, estuary,

and bay along the Bohai Sea coast, northeastern China. Appl. Geochem. 24, 1702-1711.

Xu, H., Paerl, H. W., Zhu, G., Qin, B., Hall, N. S., Zhu, M., 2017. Long-term nutrient trends and harmful cyanobacterial bloom potential in hypertrophic Lake Taihu, China. Hydrobiologia. 787, 229-242.

Yu, R., Flanders, J., Mack, E. E., Turner, R., Mirza, M. B., Barkay, T., 2012. Contribution of coexisting sulfate and iron reducing bacteria to methylmercury production in freshwater river sediments. Environ. Sci. Technol. 46, 2684-2691.

Zhang, H., Lyu, T., Bi, L., Tempero, G., Hamilton, D. P., Pan, G., 2018. Combating hypoxia/anoxia at sediment-water interfaces: a preliminary study of oxygen nanobubble modified clay materials. Sci. Total Environ. 637-638, 550-560.

Zhu, W., Song, Y., Adediran, G. A., Jiang, T., Reis, A. T., Pereira, E., Skyllberg, U., Björn, E., 2017. Mercury transformations in resuspended contaminated sediment controlled by redox conditions, chemical speciation and sources of organic matter. Geochim. Cosmochim. Acta. 220, 158-179.

723 **Graphical abstract**

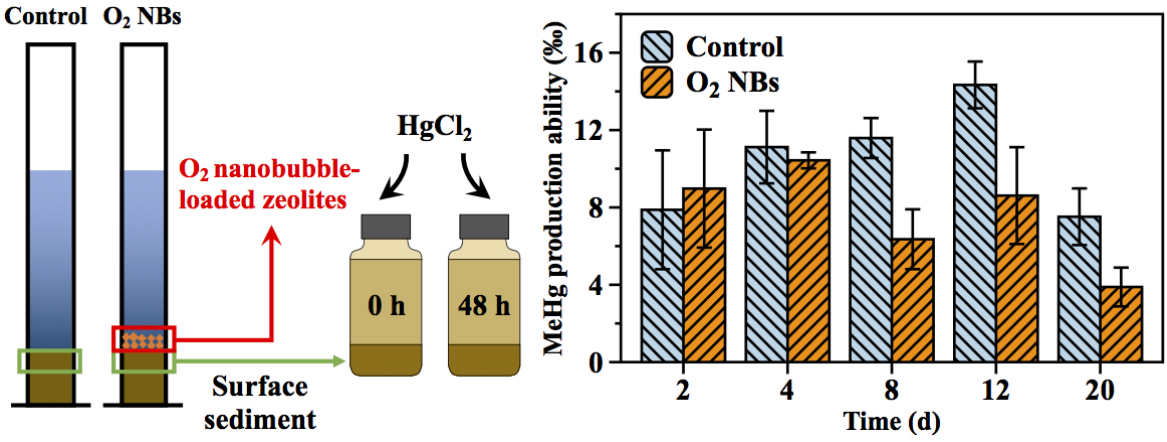

724